Molecular Dynamics Simulations of Prostaglandin Endoperoxide H Synthase-1. Role of Water and the Mechanism of Compound I Formation from Hydrogen Peroxide

R. I. Cukier* and S. A. Seibold

Department of Chemistry, Michigan State University, East Lansing, Michigan 48824-1322

Received: May 16, 2002; In Final Form: September 23, 2002

Molecular dynamics (MD) is used to study the resting state and hydrogen peroxide-bound state of Prostaglandin endoperoxide synthase-1 (PGHS-1). A water molecule, initially relatively far from the heme iron in the ferric Fe(III) oxidation state, becomes its sixth ligand. As the dynamics proceeds, this water (WL) remains close to the Fe and it hydrogen bonds to other waters. Trees of hydrogen-bonded waters form that extend from WL to the bulk solvent mainly on the distal side of the heme. WL also hydrogen bonds to typically two other water molecules in the direction away from the bulk solvent. Mutation of WL and a water hydrogen bonded to it to form H_2O_2 permits study of a mechanism for the formation of the catalytically active compound I (an Fe═O ferryl intermediate). In typical peroxidases, a conserved cationic histidine may be the source of a proton to transfer directly to hydrogen peroxide and initiate compound I formation. We find that the distal histidine of PGHS-1 moves sufficiently far from H_2O_2 that this direct mechanism cannot operate. Instead, the histidine hydrogen bonds through the imidazole's ϵ Nitrogen to the oxygens of the D-propionate of the heme. In turn, this propionate hydrogen bonds to a water that can also hydrogen bond to the Fe-bound H_2O_2. Based on this geometry, a mechanism for compound I formation is suggested that may operate at low pH where the distal histidine should be in its cationic state.

I. Introduction

Prostaglandin endoperoxide synthase-1 (PGHS-1) catalyzes the committed step in prostaglandin and thromboxane synthesis (hormonally active compounds). PGHS-1 performs both peroxidase and cyclooxygenase chemistry by interacting with the 15-hydroperoxyl group of prostaglandin G_2 (PGG_2), generating the final product, prostaglandin H_2, and an amino acid-based radical (a tyrosyl radical) that subsequently catalyzes the cyclooxygenase activity.[1−3] This latter event supplies more PGG_2 for subsequent peroxidase activity. The peroxidase and cyclooxygenase activities occur at physically distinct sites in the enzyme. PGHS-1 (and its isoform PGHS-2) are important pharmacologically because both isoforms are targets of aspirin and other nonsteroidal anti-inflammatory drugs.[4−6]

The peroxidase site of PGHS-1 consists of a heme group and a set of characteristic distal amino acids. The substrate is positioned on the distal side close to the Fe (opposite to a proximal, covalently bound histidine). The PGHS-1 peroxidase site shares many similarities with heme peroxidases[7−9] such as horseradish peroxidase (HRP), cytochrome *c* peroxidase (CCP), and myeloperoxidase. These peroxidases use hydrogen peroxide as a substrate. The peroxidase site's function is to transform a peroxide, positioned close to the Fe (ferric) heme, to the catalytically active compound I, an Fe═O ferryl intermediate, which is two oxidation states above the ferric resting state (cf. Scheme 1).[9−13] Hydrogen peroxide is also a substrate for PGHS-1 but exhibits about a 100−1000-fold lower secondary rate constant for compound I formation than its native substrate, PGG_2, or other hydrophobic alkyl hydroperoxides such as 15-hydroperoxyeicosatetraenoic acid (15-HPETE).[14] Interestingly, ethyl hydrogen peroxide is also a substrate, and its reactivity approaches that of the native substrate. In this work, we present a molecular dynamics (MD) study of the resting and hydrogen peroxide substrate states of PGHS-1, with the goals of investigating the geometry of the resting state, the presence and stability of waters around the heme and nearby residues, and the mechanism of hydrogen peroxide heterolytic cleavage to form compound I.

Crystallographic studies of heme peroxidases have shown the presence of waters in the distal active site.[8,15] These waters are thought to be ordered and may play a role in the structural stability and conformational communication between distal and proximal sides of the heme. For the ferric Fe(III) oxidation state, there is a particular water that is close, though not covalently bound, to the Fe. Of course, substrates must enter and leave the region of the active site, so there needs to be a combination of water persistence and mobility to accomplish the substrate-to-product transformation. Crystallography can give only a "snapshot", whereas molecular dynamics simulations can provide dynamical information. Collins et al.[16] used MD to examine the binding, stability, and geometry of both the resting and peroxide-bound intermediate state of CCP. They found that the crystallographic waters in the resting state are quite stable, with one being tightly bound to the heme Fe. In a short (20 ps) run utilizing the peroxide-bound intermediate, it was found that the peroxide binding is dominated by end-on versus bridged oxygen distances to the Fe and that the peroxide oxygen forms a stable hydrogen bond with a proximal (neutral) histidine. In more recent work, Filizola and Loew examined[17] similar issues for horseradish peroxidase isoenzyme C (HRPC). They carried out their simulations with the distal histidine cationic and neutral and extended the time regime to 1 ns. They still find stable networks of the crystallographic waters in the distal binding pocket and that the distal histidine is hydrogen bonding to a peroxide oxygen for both protonation states of this histidine. On the basis of the geometry of the Fe−H_2O_2 complex, they suggested a mechanism for compound I formation. When the

10.1021/jp021232i CCC: $22.00
Published on Web 10/30/2002

SCHEME 1: Formation of Compound I in a Heme Peroxidase

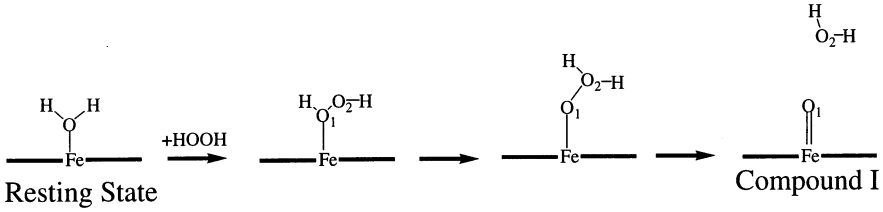

distal histidine is cationic (N_ϵ and N_δ of the imidazole ring are protonated), it can act as a proton donor to the terminal peroxide oxygen (O2). They also found a crystallographic water is positioned to act as a proton acceptor from the hydrogen of the other peroxide oxygen (O1). The combination of proton donation to O2 and proton abstraction from O1 to a water can lead to O1−O2 bond breaking and the formation of compound I. Their simulations are carried out by solvating the protein with a shell of waters that are constrained harmonically, to prevent their evaporation. One anticipates that such simulations will emphasize the stability of the water networks somewhat.

Banci et al.[18] simulated the resting state of CCP and a model they constructed of HRPC and their interactions with a phenolic substrate. In these relatively short (∼100 ps) simulations, they also find that the crystallographic waters on the distal side remain relatively well ordered and form an extensive hydrogen-bonded network, with the water close to Fe being quite rigid. De Gioia and Fantucci[19] simulated CCP and *Artromyces ramosus* peroxidase in the resting and hydrogen peroxide-bound states. They find that some of the waters are relatively fixed, in particular one that is close to the Fe, whereas others are more mobile. Here, in addition to end-on coordination of the hydrogen peroxide for significant times, it can take on an outer-sphere coordination (no longer in the heme coordination sphere) configuration.

In the MD simulations described in this work we first focus on issues pertaining to the resting state of the enzyme. In particular, we examine the ability of oxidized PGHS-1 (ferric iron) to bind a water molecule, because there is spectroscopic evidence that water does form the sixth ligand to the heme Fe in PGHS-1.[20] Our results show that a water (referred to as WL) does become associated with the Fe and remains there for the MD simulation time. The use of waters from the crystal structure (which does not confirm a water close to the Fe) versus waters introduced into the protein by an algorithm that places the protein on a water lattice and excludes protein-water overlaps (which also does not predict a water close to the Fe) does influence when ligation occurs. The formation and stability of water structures leading from the ligated water to the bulk solvent is then investigated. Networks of hydrogen-bonded water molecules are found that extend in both directions from WL. In one direction, these lead from WL to the bulk solvent, which is just a few angstroms from the exposed heme in PGHS-1. In the other direction, WL is typically hydrogen bonded in a chain structure to two waters.

Once water structures have been established in the simulation, a substrate hydrogen peroxide is introduced and its stability and geometric fluctuations are investigated. About half of the time, end-on configurations are found, and they are connected by configurations of more equal Fe−oxygen distances due to a rocking motion of the hydrogen peroxide. Our simulation has all the histidines cationic, including the distal histidine, His207. The use of a cationic His207 results in its movement sufficiently far from the heme Fe that a Filizola and Loew[17] type mechanism of compound I formation that requires it to be close to the peroxide is not viable. Instead, what we find is that His207 is strongly and persistently hydrogen bonded to the oxygen atoms of the heme's D-propionate. In our simulations, the D-propionate is often hydrogen bonded to a water, and this water, in turn, is often hydrogen bonded to the hydrogen peroxide. On the basis of this geometric arrangement, we suggest a mechanism for compound I formation that invokes a proton shuttle stretching from the cationic His207 to the hydrogen peroxide. The His207 donates a proton to a propionate oxygen that can then be transferred to a hydrogen-bonded water. This proton on H_3O^+ then can serve to protonate the O2 (terminal) peroxide oxygen. Because the O1 of the peroxide is always hydrogen bonded through its hydrogen to other waters, these other waters can act as proton acceptors and again lead to O1−O2 bond dissociation, as suggested by Filizola and Loew. The key role in compound I formation played by the His207 is maintained in this mechanism and is in accord with the results of mutagenesis experiments that show a drastic loss in the rate of compound I formation when this histidine is mutated.[21]

The plan of the rest of this work follows. In section II we describe the MD program we developed and the analysis program we wrote to find and catalog networks of hydrogen-bonded waters. Section III presents the results of these simulations and section IV analyzes them. In section V we summarize our conclusions.

II. Methods

The molecular dynamics simulation was carried out by modifying our existing MD code to incorporate proteins and other large solutes. The GROMOS[22] force-field was used for the residues and solvent water. Modifications to the heme in the GROMOS force-field were made to create a ferric Fe(III), as discussed below. A combination of a cell index method with linked lists[23] and a Verlet neighbor list[24] was implemented to provide linear scaling with the number of atoms in the pair list routine, essential for the large systems considered here. For the Verlet neighbor list, the outer distance is $r_l = 12.8$ Å and the inner distance is $r_c = 10.0$ Å. The update of the pair list is done whenever any atom moves a distance greater than $0.5(r_l - r_c)$, leading to updates roughly every 30 steps. The electrostatic interactions were evaluated using the charge-group method, to be consistent with the parameterization of the GROMOS force field. In the GROMOS methodology, a twin-range method is used whereby the electrostatic interactions are kept fixed for a certain number of MD steps before the update of the atom positions. We used, instead, the above-noted Verlet neighbor list update procedure. The SHAKE algorithm[22] was used to constrain bond lengths, permitting a 2 fs time step. Periodic boundary conditions are used. The simulation was carried out at constant NVT with velocity scaling to control the temperature to around 300 K. Numerous start-up protocols were used for reasons discussed in section III. In each start method, we create a face-centered cubic lattice of water molecules and center the protein in the simulation cell. The

waters that overlap the protein, on the basis of their (oxygen) to protein atom distance $r_{ij} < \sigma_{ij}$, with σ_{ij} the corresponding van der Waals radius, are discarded. The simulation is started with the protein cold, and we let the solvent heat the protein as the solvent molecules equilibrate to each other and the protein. Alternatively, the water also starts at zero degrees and is gradually heated with the protein to 300 K over 1 or 10 ps. Another set of initiation runs constrained the protein (non hydrogen) atoms with a harmonic potential with force constant 30 (kcal/mol)/Å^2 for 1, 5, or 10 ps, after which the constraints were gradually released. Combinations of temperature and constraint protocols were also tried. The simulations with the water ligand were carried out for approximately 1 ns. Once we selected a configuration (at 420 ps) to form the hydrogen peroxide, the peroxide simulation was carried out for 720 ps.

The starting configuration of prostaglandin H2 synthase-1 (PGHS-1) was obtained from the Protein Data Bank (PDB) entry code 1CQE.[25] This 3.1 Å resolution structure has 551 residues that are sufficiently resolved to be included in the simulation. The simulation was carried out on the monomer, as the issues discussed here focus on the access of water to the heme, and the water channel is opposite to the dimer interface. Some strains in the crystal structure were evident, and they were relaxed by using a steepest descent energy minimization scheme before the MD was started. The protein simulated had a total of 5437 atoms, including the polar hydrogens that were added by use of the Babel program.[26] After overlapping waters were removed, there were 19 798 water molecules left in the simulation box. The simulation box side is 88.8 Å, and the largest dimension of PGHS-1 is 73 Å, leaving about 30 Å between protein molecules in neighboring cells. The large number of waters used facilitates investigation of the transport of water in to and out of the heme pocket.

A force field for the ferric heme was synthesized from the literature and used to modify the ferrous heme in the GROMOS force-field database. A number of studies have been devoted to constructing a ferric heme force-field, the critical issue being the charges on the Fe and the surrounding atoms. A consensus force-field was used where the charge on the Fe is taken as +1.0 and each pyrrole nitrogen has 0.0 charge. The charges on Fe(III) used in various simulations[16,18,27] range from 0.8[27] to 1.25.[16] Iron van der Waals parameters were obtained from the work of De Gioia and Fantucci[19] where they were designed to reproduce the experimental Fe−H_2O geometry observed in model protoporphyrin water complexes.

Parameters for hydrogen peroxide are given in Table 1. The charges are obtained from the Merck force-field.[28] The dihedral angle was modeled with the potential

$$V_{\mathrm{dih}} = \sum_{n=1}^{3} V_n \cos(nx)$$

which yields a trans barrier of 386 cm^{-1} and a cis barrier of 2460 cm^{-1} with two minima at +111.5° and −111.5° referenced to the trans barrier placed at 0°.[29] The equilibrium angle and force constant values[30] for the HOO and OOH bond angles are also given in Table 1. The hydrogen peroxide was formed by taking two hydrogen-bonded waters at an appropriate MD step and mutating them by changing the charges of two hydrogen atoms (one from each water) from 0.41 to 0.0, of the other two hydrogens from +0.41 to +0.4, and of the oxygen charges from −0.82 to −0.4 and reducing the O−O van der Waals interaction to zero. The O−O bond length was "reeled in" from the initial distance of two hydrogen-bonded waters, about 2.8 Å, to the equilibrium distance of 1.45 Å.[30] The changes were carried out over a 3 ps time interval by linearly interpolating all the quantities between their respective initial and final values.

TABLE 1: Force-Field Parameters for Ferric Heme and Hydrogen Peroxide

van der Waals Parameters[a]			
		A [(kcal/mol)/Å^{12}]	B [(kcal/mol)/Å^6]
Fe		10389.5	288.3
Partial Charges (Electron Units)			
	Fe[b]		+1.0
	N[b]		+0.0
	H (peroxide)		+0.4
	O (peroxide)		−0.4
Bonding Parameters for HOOH			
		equilibrium value	force constant
bond distance	HO	1.0 Å	∞[c]
bond distance	OO	1.45 Å	1000.0 (kcal/mol)/Å^2
bond angle	HOO	110°	100.0 (kcal/mol)/rad^2
dihedral angle	HOOH	$V_1 = 993$ cm^{-1}, $V_2 = 636$ cm^{-1}, $V_3 = 44$ cm^{-1}	

[a] $V_{\mathrm{nb}}(rij) = A_{ij} r_{ij}^{-12} - B_{ij} r_{ij}^{-6}$ with $A_{ij}(B_{ij})$ the geometric means of A_i and $A_j(B_i$ and $Bj)$. [b] All other heme charges are the same as the GROMOS ferrous heme. [c] Constrained.

A program to construct hydrogen-bonded water "trees" emanating from a "root" water was developed. The multifunctionality of water and its donor/acceptor character as a hydrogen bonder lead to the tree structure. All waters within 8 Å of the heme Fe were written out every tenth MD step (20 fs). A "root" water is picked — for example, the water that we find ligated to the Fe. All waters (defined as level 1 waters) hydrogen bonded to the root (defined as level 0) are stored, and the root is removed from the list of possible hydrogen bonders. Each level 1 water is, in turn, now considered a root. All waters hydrogen bonded to each of these level 1 waters are stored in level 2, and all level 1 waters are removed from the list of possible hydrogen bonders. This procedure is continued recursively. Picking a desired number of levels, N_{lev}, will then produce, for all the MD steps considered, trees of hydrogen-bonded waters of *at least* length N_{lev}. The criterion for hydrogen-bond formation was varied from "easy", WOa−WOb distance between the oxygens of waters a and b $d_{\mathrm{WOaWOb}} < 3.5$ Å, to "hard", $d_{\mathrm{WOaWOb}} < 3.0$ Å and the WOaHaWOb angle, A_{WOaHaWOb}, satisfying $145° < A_{\mathrm{WOaHaWOb}} < 180°$ when the hydrogen covalent bond is in water a and similar when the covalent bond is in water b.

III. Results

A. Resting State. The role of water as a potential sixth ligand of the heme Fe was assessed by starting the simulation from two types of initial conditions. First, we placed the protein over a lattice of waters and eliminated the waters that overlapped the protein by using the criterion that the distance between a water oxygen and a residue (or heme) atom was less than the van der Waals radius obtained from the corresponding water oxygen and residue or heme atom's van der Waals radii. This left four waters within an 8 Å radius sphere of the Fe (along with others farther away). We shall refer to this situation as the MD initial condition. The placement of these waters was not optimized; they are part of the original water lattice and show that the crystal structure is relatively open in this region. Alternatively, we replaced these four waters by the three waters that were found to lie within an 8 Å radius sphere of the Fe in

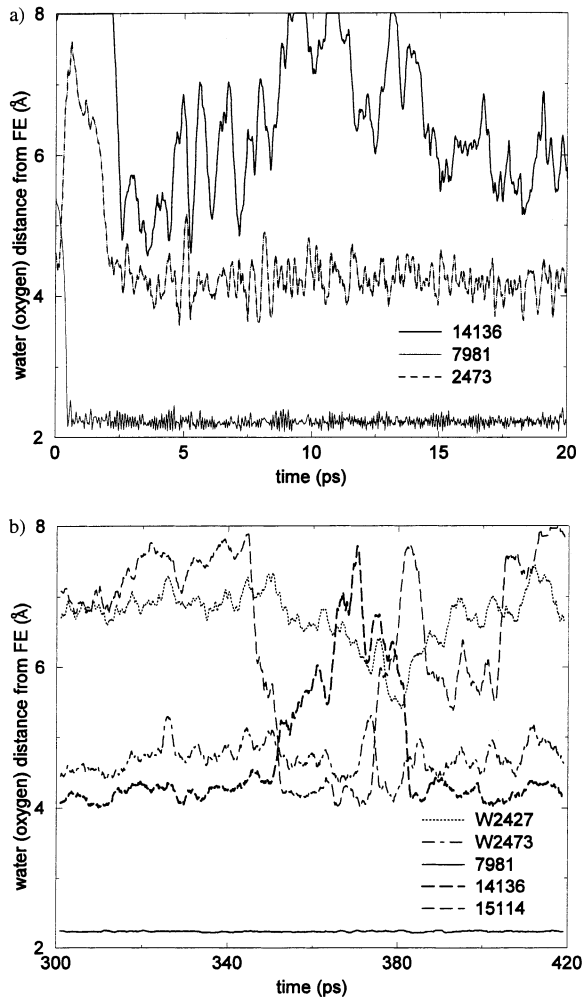

Figure 1. Distance between the oxygen of some waters and the Fe of heme for waters within 8 Å of the Fe versus time. (a) The first 20 ps run. Of the four waters W2167, W2473, W7981, and W14136 that are within 8 Å of the Fe initially, using our MD initial condition (see text), W7981 rapidly (in about 0.4 ps) ligates to the Fe, suggesting that the Fe is six-coordinate when it is in the ferric oxidation state. W2167 wanders outside the 8 Å sphere around 10 ps and is not shown in the figure, for clarity. (b) The interval between 300 and 420 ps. The W7981 is still ligated to Fe, and W2473 and W14136 are still present and form hydrogen bonds with W7981.

the crystal structure. We refer to this situation as the XRAY initial condition. Figures 1 and 2 plot some of the waters that are within 8 Å of the Fe as a function of time. (We stress that the numbering schemes of the waters for the MD and XRAY initial conditions are independent.) These waters will be referred to as "inside" waters. Waters that move out of this sphere are indicated by the 8 Å line. Not all the waters are displayed, for clarity, because some move in for only a very short time period. For the MD initial condition, one of the waters within 8 Å became ligated to the Fe within about 0.4 ps, as shown in Figure 1. For the XRAY initial condition, Figure 2b shows that it took about 50 ps to ligate a water. A number of simulation startups were tried by constraining the (non-hydrogen) protein atoms for varying lengths of time before gradually releasing them and by ramping up the solvent temperature from low to ambient, and combinations of these conditions. All methods led to a water becoming the sixth ligand, with water-ion ligation times between the above-mentioned 0.4 ps and about 92 ps. Thus, we conclude that there is a strong propensity to form six-coordinate water for the ferric oxidation state.

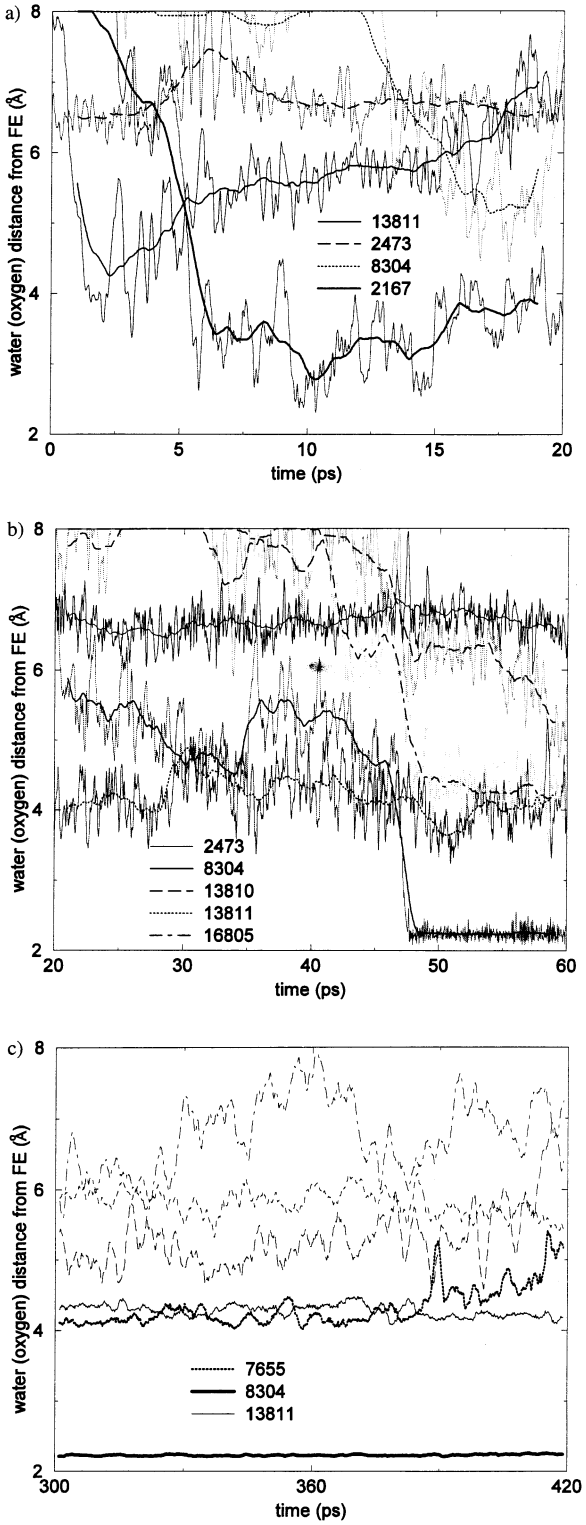

Figure 2. Same as Figure 1 for the XRAY initial condition (see text). (a) The first 20 ps. Of the three waters initially present, W2473, 2167, and 7981, two, W7981 and W2473, eventually leave the 8 Å inside region and two, W8304 and W13811 enter it. Panel b shows that W8304 enters the inside region, becomes trapped by the Fe, and ligates to it. The indicated lines on the figure are 0.2 ps moving averages. Panel c shows that considerably later W8304 is still ligated to the Fe. It remains ligated for the entire MD run. The W7655 is hydrogen bonded to W8304, and the two will be used to form a hydrogen peroxide molecule. The lines on the figure are 0.2 ps moving averages.

When the XRAY initial condition is used, of the original three crystal waters (W2167, W2473 and W7981), two remain (W2473 and W2167) and two new (W8304 and W13811) move

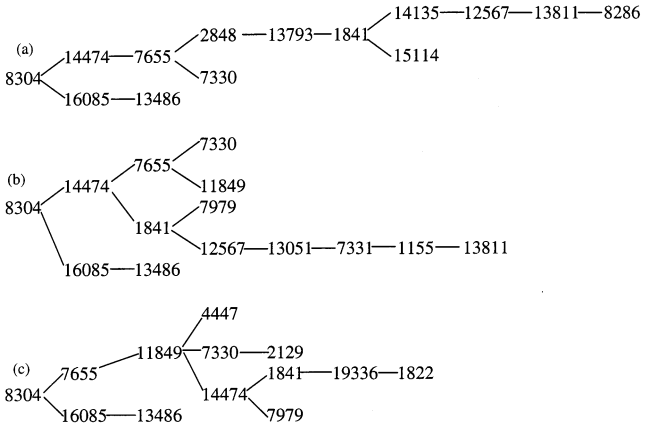

Figure 3. Typical trees of simultaneously hydrogen-bonded waters at selected times. The "root" is taken as the water ligated to the Fe (WL = W8304 here), and all waters within 8 Å of the Fe are searched for hydrogen bonding. The waters on the lower branch are going away from the bulk (W16085 and W13486). Those on the upper branch are going toward the bulk. In (c) W7655 has exchanged places with W14474 in (a) and (b). Although the waters are more confined than in the bulk by the surrounding residues and heme, there can be numerous branches in the trees. The easy hydrogen-bonding criterion (see text) of oxygen−oxygen distances all smaller than 3.5 Å was used to generate these picture.

Figure 4. Hydrogen-bonded network of waters corresponding to Figure 3c. The larger (stick) waters correspond to these waters. The smaller (line) waters are those within 12 Å of the Fe without regard to their hydrogen-bonding status. The heme and several residues, in particular the proximal histidine (down) and the distal histidine (up), are also shown for purposes of orientation. The hydrogen-bonded network funnels down from the bulk solvent (left side) to extend to WL (the Fe ligated water) and further in a linear fashion into a relatively hydrophobic region.

in and persist in the first 20 ps run (Figure 2a). Figure 2b shows the ligation of W8304 (not one of the original ones within 8 Å). In the 40 ps of Figure 2b, 36 distinct waters are found to spend some time inside. Of these, five (W2473, W8304, W13810, W13811, and W16805) are "persistent", spending most of their time inside. In Figure 2c the state between 300 and 420 ps is shown. W8304 has persisted until this time interval and continues to do so with its oxygen around 2.2 Å from the Fe. Six waters are displayed, and note that W13811 has also persisted from the beginning. The W7655 is, as we shall see, hydrogen bonded to W8304 and will be used to form hydrogen peroxide (vide infra). The W8304 stays ligated to the Fe for the roughly 1 ns that we have run the simulation. The same is true of the water that is ligated to Fe using the MD initial condition. We will refer to the ligated water as WL.

The initial number of inside waters, three using the XRAY and four using the MD initial condition, increases to about 10−15 at any given time after an initiation period. In any 40 ps (120 ps) interval, there are around 35 (60) distinct waters that spend some time inside the 8 Å sphere around the heme Fe. These features suggest that the WL can act as a "recruiter" for other waters and potentially form networks centered on it. Note in PGHS-1 the heme is quite exposed to the solvent,[25] which lets us explore the flux of water in and out of the heme pocket in a reasonable amount of computational time. In the Methods section, an approach to constructing hydrogen-bonded water trees was described. Figure 3 is a diagram of some typical trees we generated from the MD data in the same time window as in Figure 2c. The trees are generated using the "easy" criterion $d_{\mathrm{WOaWOb}} < 3.5$ Å. The "root" of the tree, W8304, was chosen as WL. It is clear that long runs of simultaneously hydrogen-bonded waters exist. They connect the bulk solvent to WL. Note that the waters far from WL that are heading into the bulk are not themselves very ramified in this display (they do not appear to have a highly hydrogen-bonded structure); that is because we have only considered waters within 8 Å of the heme Fe in our search for trees. Increasing the search radius does show that expected behavior, but the trees become rather unwieldy to display. There is a switch in pattern between (a) and (b) and (c) in Figure 3 whereby 8304−14474−7655−11849 becomes 8304−7655−11849−14474. The interchange of WL's hydrogen bond partner shows the lability of the waters that WL recruits. These exchanges occur on roughly a 20 ps time scale. By writing out all trees whose length (N_{lev} of the Methods section) is six or greater, we can get a sense of the persistence of such chains. For the easy hydrogen-bond criterion, trees of at least length six occur about 25% of the time. If we use the "hard" condition ($d_{\mathrm{WOaWOb}} < 3.0$ Å and $145° < A_{\mathrm{WoaHa(b)WOb}} < 180°$), this number drops to about 7% of the time. A linear arrangement of six hydrogen-bonded waters provides a path of around 20 Å, giving ample room to connect bulk with the ligated water, WL. Using the easy criterion, trees of at least length three are present about 90% of the time, and trees of length two always exist, with W8304 hydrogen bonded to two other waters (that exchange).

For the hard condition, 5% of the time there are trees of only length one. That is, only W8304 forms a continuous hydrogen-bonded tree with a neighboring water. (Of course, this does not mean that the other waters are not forming hydrogen bonds—we always start the tree from WL, the Fe-ligated water.) Thus, WL forms two or more strong hydrogen bonds 95% of the time. Nevertheless, as the figures show, WL eventually exchanges its neighboring waters. The tree in Figure 3c is displayed in Figure 4, with these waters represented in stick mode. The line waters shown are those within 12 Å of the Fe. The heme and several residues, in particular the covalently bonded, proximal His388 (down) and the distal His207 (up), are displayed for purposes of orientation. The hydrogen-bonded network funnels down from the bulk solvent (left side) to extend to WL and further in a linear fashion into a relatively hydrophobic region. The W16085 and W13486 are those extending to the right of WL. Note that, at any time, some of the line waters are hydrogen bonded; because those are mainly bulk ones and form "typical" solvent hydrogen bonds, we have not indicated them. Rather, we focus on the patterns of hydrogen bonds for waters associated with the heme Fe.

SCHEME 2: Crystallographic Water in Position to Hydrogen Bond to Tyr504 and His388

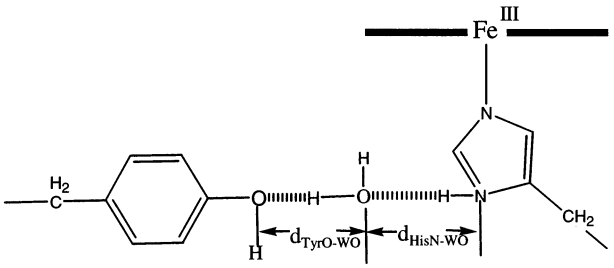

Analogous patterns to the XRAY initial condition data just discussed occur for the MD initial condition. Initially, all four waters start on the distal side of the heme plane with the closest W2473 being 4.6 Å away from the Fe. These waters are present because the residue and heme positions provide sufficient space that they were not eliminated by van der Waals overlap with the initial lattice of waters. The W7981, starting 5.4 Å away from the Fe, rapidly ligates to the Fe, as shown in Figure 1a, and remains there for all of the MD run. The water W2167 originally present stays around 7 Å away in the first 20 ps, moves away, and then never comes closer than 8 Å for the entire run. Two of the original waters, W2473 and W14136, remain close and become part of the waters recruited by W7981. In Figure 1b, the distance data for the interval 300−420 ps are displayed where W7981, W2473, and W14136 form a fluctuating hydrogen-bonded pattern. Note the large excursion of W14136 that takes it quite far away from W7981 for a while. The same kind of hydrogen-bonded trees form as discussed for the XRAY initial condition simulations.

The water labeled W2473 was positioned in the X-ray structure to span the proximal His388 and Tyr504, according to the pattern shown in Scheme 2.[25] We monitored the position of W2473 relative to these residues to see the persistence of this double hydrogen-bonding pattern. Figure 5 shows the His388 N_δ to W2473 oxygen distance $d_{\mathrm{HisN-WO}}$ and Tyr504 phenolic oxygen to W2473 oxygen distance $d_{\mathrm{TyrO-WO}}$, for two time intervals. The initial X-ray structure has $d_{\mathrm{TyrO-WO}} = 2.76$ Å and $d_{\mathrm{HisN-WO}} = 2.75$ Å. The Tyr504-W2473 hydrogen bond is very persistent and strong, whereas the His388−W2473 hydrogen bond is breaking and re-forming. The distance $d_{\mathrm{HisN-WO}}$ at earlier times is on average longer than at later times. Because there is a distinct anticorrelation in the distances $d_{\mathrm{TyrO-WO}}$ and $d_{\mathrm{HisN-WO}}$, it appears that the two residues are separated by a relatively stable distance.

The MD simulation exhibits a local movement of residues around the heme that will be important to our discussion of the mechanism for compound I formation. In Figure 6, we display the orientation and distances of the His207 C_α, and the imidazole N_ϵ and N_δ atoms from the Fe. The initial (Figure 6a) and 13 ps (Figure 6b) configurations for the MD initial condition data are displayed. It is clear that the imidazole ring is rotating relative to the Fe, bringing the ϵ nitrogen farther away from the Fe than a distance where it could participate directly in compound I formation. Note that the C_α only moves 1 Å in 13 ps. This indicates that most of the movement of the His207 is the rotation of the imidazole ring. Figure 6c displays analogous information for the XRAY initial condition, as well as the positions of the initially present waters, at an MD time of 0.4 ps. The water W2167 that is close to the imidazole ring initially (the water's oxygen is 3.3 Å from the ϵ nitrogen) comes even closer to 2.77 Å. In both cases, strong oxygen−proton interactions can occur and produce a rapid rotation of the imidazole ring.

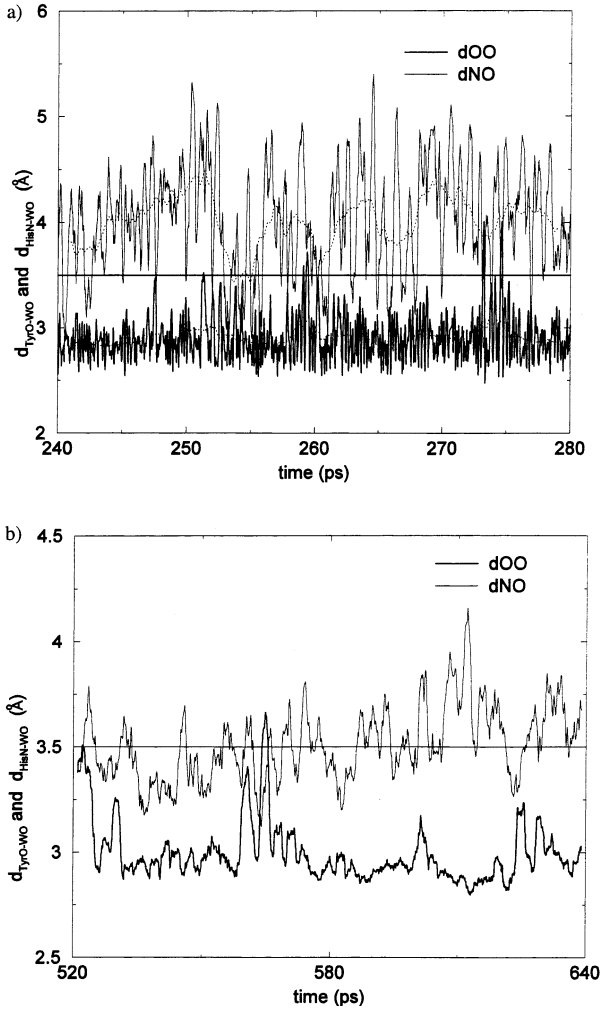

Figure 5. Distances $d_{\mathrm{TyrO-WO}}$ and $d_{\mathrm{HisN-WO}}$ between, respectively, Tyr504's phenolic oxygen and W2473's oxygen and His388's ϵ nitrogen and W2473's oxygen plotted for two different time regimes. The X-ray structure positions W2473 between these residues, with the oxygen forming hydrogen bonds to both residues. The simulation shows that W2473 remains strongly hydrogen bonded to the tyrosine, but the hydrogen bond to the histidine is there only part of the time. The top panel solid lines are the data written out every 20 fs, and the dotted lines are 2 ps moving averages. The bottom panel only displays the 2 ps moving average data.

The α helix that forms part of the heme dome stays quite stable during the simulation. We investigated this by evaluating the time-averaged distance between pairs of C_α atoms of two amino acids in the same helix, relative to their initial distances, $(1/T)\int_0^T r_{jk}(t)\,dt - r_{jk}(0)$, as given in Table 2. The data over the first 20 ps shows that the greatest initial movement is in the Ala202−His207 distance. The data from 500 to 620 ps shows that there are only small oscillations about the initial distances. Examining all the data over the 1 ns run gives essentially the same results. Thus, although the helix above the heme has shifted somewhat relative to the crystal structure, the helix stays intact and has essentially the same relative geometry.

B. Hydrogen Peroxide Substrate. Having equilibrated water to the heme pocket of PGHS-1, we now turn to introducing a simple peroxidase substrate, namely H_2O_2. Because it would be difficult on a MD time scale to diffuse in a substrate, especially once waters have been allowed to permeate the active site, we adopt the following strategy to make the peroxide. The W8304 that is ligated to Fe, for the XRAY initial condition, and a neighboring hydrogen-bonded water are "mutated" to

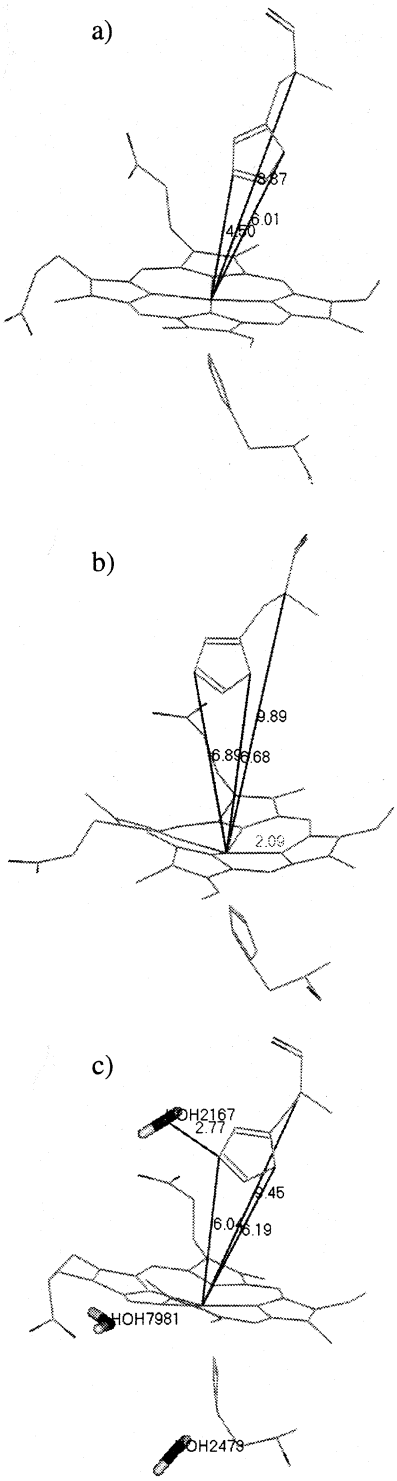

Figure 6. Distances of the C_α and the imidazole N_ϵ and N_δ atoms of His207 relative to the heme Fe: (a) initial, X-ray, coordinates, (b) after 13 ps of MD for the MD initial condition, and (c) after 0.4 ps of MD for the X-ray initial condition. In (a) the ϵ nitrogen is 4.5 Å from the Fe and it is 6.89 Å away in (b) and 6.04 Å in (c). The imidazole ring rotates (the N_δ movement is much smaller) relative to the Fe. The movement of the C_α atom of His 207 is 0.6 Å in (c) and 1 Å in (b) relative to the initial position.

hydrogen peroxide. Thus, the W7655 that is hydrogen bonded to W8304, as displayed in Figure 3c, is used to create a H_2O_2 molecule. The protocol for carrying out this transformation is discussed in the Methods. Once the H_2O_2 is formed, it is allowed to interact with its surroundings for the remainder of the simulation (600 ps). Initially, the HOOH dihedral angle swings

TABLE 2: Time-Averaged Distance between Indicated Residues, Relative to Their Initial Distances of the Heme Dome α Helix Region[a]

begin residue		end residue		distance (Å)
ALA	202	GLN	203	0.0552417
ALA	202	HIS	204	−0.244884
ALA	202	PHE	205	0.0722862
ALA	202	THR	206	0.309979
ALA	202	HIS	207	0.835154
ALA	202	GLN	203	−0.0354824
ALA	202	HIS	204	−0.10361
ALA	202	PHE	205	0.314474
ALA	202	THR	206	0.0915894
ALA	202	HIS	207	0.550611
ALA	202	GLN	203	−0.0274214
ALA	202	HIS	204	0.0444405
ALA	202	PHE	205	0.194964
ALA	202	THR	206	−0.0247029
ALA	202	HIS	207	−0.275727

[a] First (second) [third] set is average over the initial, 0−20 (300−420) [500−620] ps.

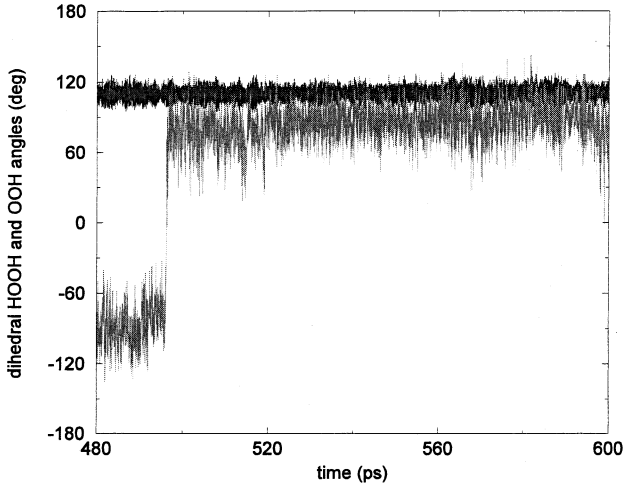

Figure 7. HOOH dihedral angle (light line) and the HOO and OOH angles (dark lines) of H2O2 plotted as a function of time. The HOO and OOH angles just oscillate around their equilibrium positions. The dihedral angle exhibits a sharp transition over the trans barrier of 386 cm^{-1} (located at 0°) between its two minima around ±110°.

from one equilibrium conformer to the other at a somewhat higher rate than later on. Over a 600 ps time interval, there are 6 complete (−110° to +110°) transitions over the trans-barrier state that is located at 0°. Figure 7 shows data over a 120 ps interval where there is one transition. As with all the transitions, it is quite sharp, as expected. The other data in Figure 7 correspond to the HOO and OOH angles that exhibit small oscillations about their equilibrium positions. Which oxygen of the peroxide is closest to the Fe is of interest in defining the mechanism of compound I formation, as proposed by Filizola and Loew.[17] We investigate the issue by examining (1) the components x_{FeO1}, y_{FeO1}, and z_{FeO1} and the magnitude r_{FeO1} of the vector between O1 (the oxygen that initially is closest to Fe, as drawn in Scheme 1) and (2) the components of the intra-oxygen vector x_{O1O2}, y_{O1O2} and z_{O1O2}. In Figure 8a, we see that the O1 moves away from the Fe (the equilibrium distance is around 2.2 Å) for about 20 ps but the oxygens do not exchange their position (z_{O1O2} remains positive). The second time O1 moves away from the Fe (around 150−175 ps), z_{O1O2} does change sign, indicating an exchange of the oxygens. By happenstance, the O1−O2 orientation relative to the MD simulation box is aligned along the *z* axis so the other two

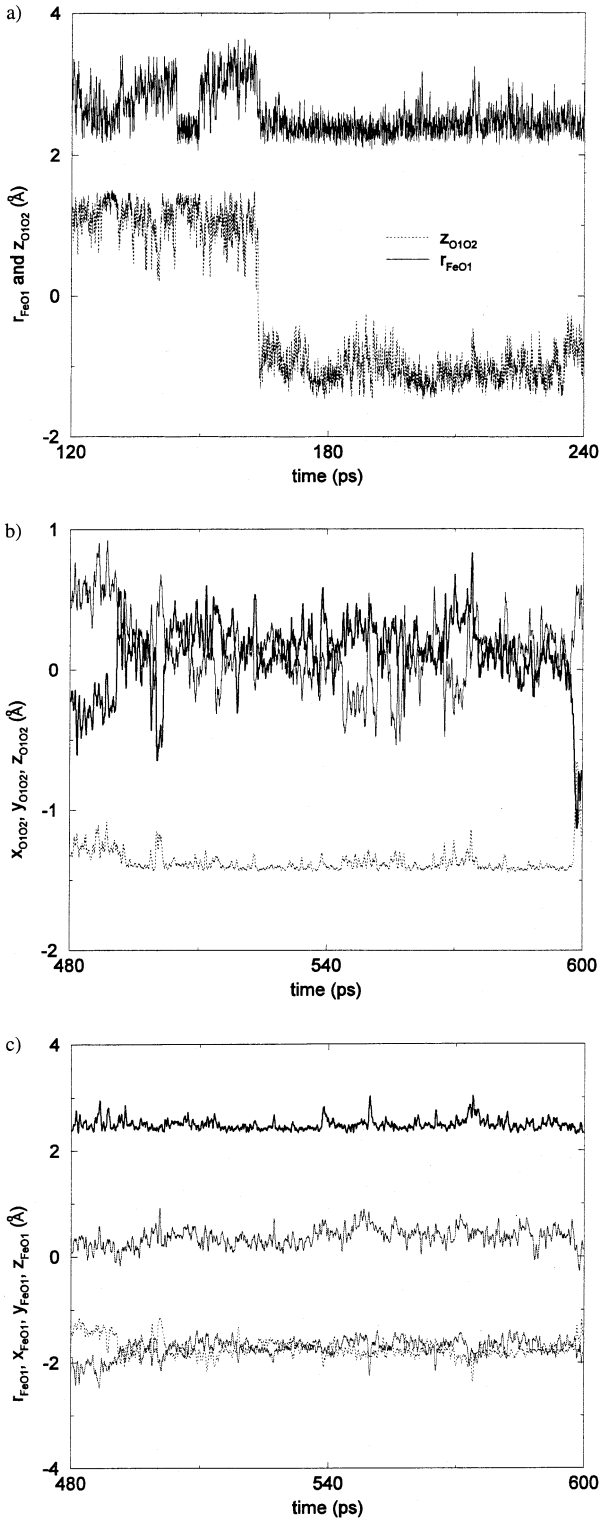

Figure 8. (a) z component of the intra-oxygen vector, z_{O1O2}, and the O1 Fe distance r_{FeO1} from 120 to 240 ps (0 is relative to the beginning of the peroxide simulation). The r_{FeO1} distance fluctuates to larger than the mean value of 2.2 Å twice, once without and once with oxygen interchange. (b) Components of the intra-oxygen vector, x_{O1O2}, y_{O1O2}, and z_{O1O2}, for 480−600 ps with a 0.4 ps moving average to smooth the data. (c) Components of and magnitude of the vector between Fe and O1, x_{FeO1}, y_{FeO1}, and z_{FeO1} and r_{FeO1} (the line fluctuating around 2.2 Å), with a 0.4 ps moving average to smooth the data.

components hardly change. In Figure 8b,c, there is evidence for, at the beginning, a flip of O1 and O2 accompanied by moderate changes in the components of the Fe−O1 vector without much change in the vector's magnitude. Around 600 ps, even the components of the Fe−O1 vector, shown in Figure 8c, hardly change, yet the O1−O2 components displayed in Figure 8b) show an interchange. Let us note that the data have been smoothed with a 0.4 ps moving average. The actual data show fluctuations of ∼0.25 Å on the scale of the 2 fs MD step. Most simulations do not capture this fast jitter because of the write interval of output. Examination of the 600 ps run shows that these oxygen−oxygen exchanges occur on average about every 100 ps. The dihedral transitions do not seem to correlate with the O1−O2 flips.

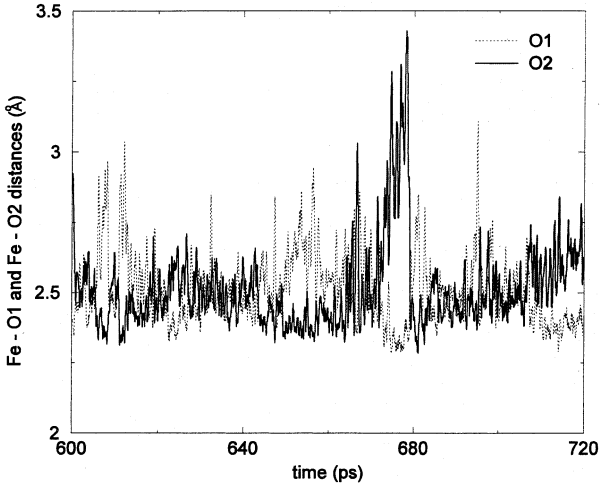

Figure 9. Distances between Fe and the two oxygen atoms of the peroxide. The data are smoothed with a 0.4 ps moving average. There are large changes in these distances, centered on the times at 660 and 680 ps. The event around 660 ps corresponds to the oxygens "rocking", whereby the O1 and O2 to Fe distances interchange. The event around 680 ps leads to an interchange of the two peroxide oxygens relative to the heme ring (cf. Figure 10).

The dynamics of the two peroxide oxygens is more fully explored by examining the Fe−O1 and Fe−O2 distances as a function of time, as displayed in Figure 9 for the interval 600−720 ps. The peroxide spends roughly equal time between "end-on" configurations where the Fe−O1 and Fe−O2 distances are rather unequal and configurations where they are relatively the same length. There are events around 650, 676, and 682 ps that are instructive to visualize. In Figure 10, panels a−c correspond respectively to these three times and display the heme, selected waters, the peroxide, and the proximal and distal histidines. We refer to the motion between panels a and b as a "rock" because the two oxygens do not exchange their positions (W7655 is on the right side of these figures). In panel c, the two bond lengths are essentially the same, but the oxygens have exchanged their position (W7655 is on the left side). Thus, in accord with the evidence from distance plots in Figures 8 and 9, the oxygen Fe distances can switch and become equal. The motion can occur by rocking or exchange.

In Figure 10a, the stick waters that are displayed are "strong" hydrogen bonds whereas the ball-and-stick ones are "weak" hydrogen bonds. The strong hydrogen bonds may be viewed as very persistent ones because, at least if we just consider chains that encompass the peroxide and the waters directly linked to it (W16085 and W6963), the data obtained from our tree algorithm indicate that this linkage can persist for time of order 50−100 ps. Examination of Figure 10b, where the Fe−O1 and Fe−O2 distances have "reversed", shows that W6963 is still hydrogen bonded to O1 and W16085 is still hydrogen bonded to O2. However, between 676 and 682 ps, there is exchange of the peroxide oxygens, associated with a large change in the Fe−O1 and Fe−O2 distances shown in Figure 9 and a change in

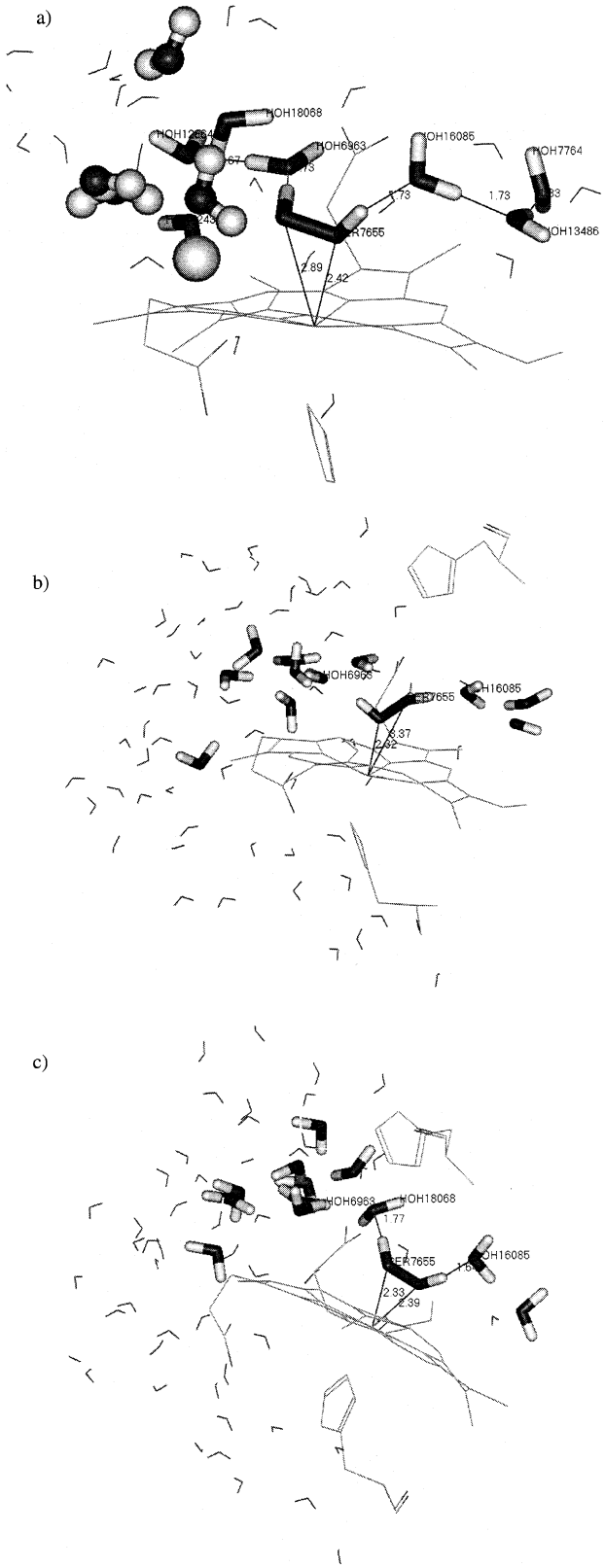

Figure 10. Plots of heme, peroxide, selected waters, and proximal (down) and distal (up) histidines. (a) At time 652 ps where O1 (unlabeled peroxide oxygen) is farther from Fe than O2 (the one labeled 7655). (b) Time 676 ps where the situation of (a) is reversed. W6963 is directly hydrogen bonded to O1 and W16085 is directly hydrogen bonded to O2 in (a) and (b). The waters displayed in (a) in stick view are strongly hydrogen-bonded ones, those in the ball-and-stick view are weakly hydrogen bonded (cf. text for definition of weak and strong hydrogen bonds). (c) Time 682 ps where it is evident that O1 and O2 exchanged their positions. The hydrogen-bonding pattern now shows that W18068 is hydrogen bonded to O1, W16085 is still hydrogen bonded to O2, and W6963 has moved one link away.

the hydrogen-bonding pattern. Now, as shown in Figure 10c, W18068 is hydrogen bonded to O1, W16085 is still hydrogen bonded to O2, and W6963 has moved one link away. Thus, the exchange of the peroxide oxygens is associated with changes in the hydrogen-bonding pattern of the waters local to the peroxide.

C. Compound I Formation. The movement of His207 away from the heme group will be important to our mechanism of compound I formation. Scheme 3 provides a potential mechanism that relies on a chain of hydrogen bonds spanning His207 to the peroxide. The energetic feasibility of the scheme will be presented in the Discussion. Here we examine the geometric feasibility. Figure 11 shows that the carboxylate oxygens of the heme's D-propionate are hydrogen bonded to the N_ϵ of cationic His207. The distances indicate that this is a strong, three-center hydrogen bond,[31] and indeed, once it is formed, this hydrogen-bonding pattern persists for the entire MD simulation. With a strong hydrogen bond of an amine−carboxylate nature, the possibility exists for proton transfer to make a neutral His207 and the carboxylic acid. In Figure 11a, the propionate's carboxylate is also hydrogen bonding to W18068 but rather weakly, as the distance is 2.44 Å. At the same instant, a hydrogen atom of W18068 is strongly hydrogen bonded (1.89 Å) to O2 of the peroxide (cf. Scheme 1). A short time later (1 ps), as shown in Figure 11b, the weak carboxylate−W18068 hydrogen bond is now strong (1.71 Å) whereas the W18068−O2 hydrogen bond is weaker (2.4 Å). This kind of motion provides a water-molecule shuttle between the propionate's carboxylate and the peroxide oxygen that can provide a proton transfer mechanism. (Because we only write out complete configuration files every picosecond, the shuttle could, and probably does, act more rapidly, on the basis of the speed of the fluctuations of the waters that clearly occur in the MD.)

There are actually two requirements for productive encounters to lead to compound I formation. In addition to the positioning of a water to hydrogen bond to both the peroxide and the carboxylate, the peroxide hydrogen bond must be from a peroxide *oxygen* to a water *hydrogen*, versus a peroxide *hydrogen* being hydrogen bonded to the water *oxygen*. Figure 10a shows an example of this latter situation with W16085's oxygen hydrogen bonded to the peroxide hydrogen H1 (cf. Scheme 1 where we use the designation O1 and H1 to refer to the peroxide oxygen being closest to the iron). A hydrogen bond of this type is not productive. Examining the statistics of hydrogen bonding shows that around 4−5% of the configurations are productive, as typified by those shown in Figure 11. That is, about 4−5% of the time there is a water positioned correctly between the propionate and the peroxide O2 to initiate compound I formation. The distance between O2 and a hydrogen atom of W18068 averages around 2.0 Å, with fluctuations between 1.75 and 2.5 Å (the hydrogen−heavy-atom cutoff distance for hydrogen bonding we use). In Figure 12 we show another configuration that shows the same pattern of His207−propionate−water−peroxide hydrogen bonding and also illustrates the feature that H1, the hydrogen of the O1, is hydrogen bonded to two waters in a strong hydrogen-bonding pattern. Thus, H1 is persistently hydrogen bonded to a least two waters, and the second water is pointed into the water pool with its transient hydrogen-bonding networks.

IV. Discussion

Optical and Raman experiments on resting-state ferrous and ferric PGHS-1 showed that the oxidized, ferric state exits exclusively as a high-spin six-coordinate structure.[20] The sixth

SCHEME 3: Proposed Mechanism for Compound I Formation[a]

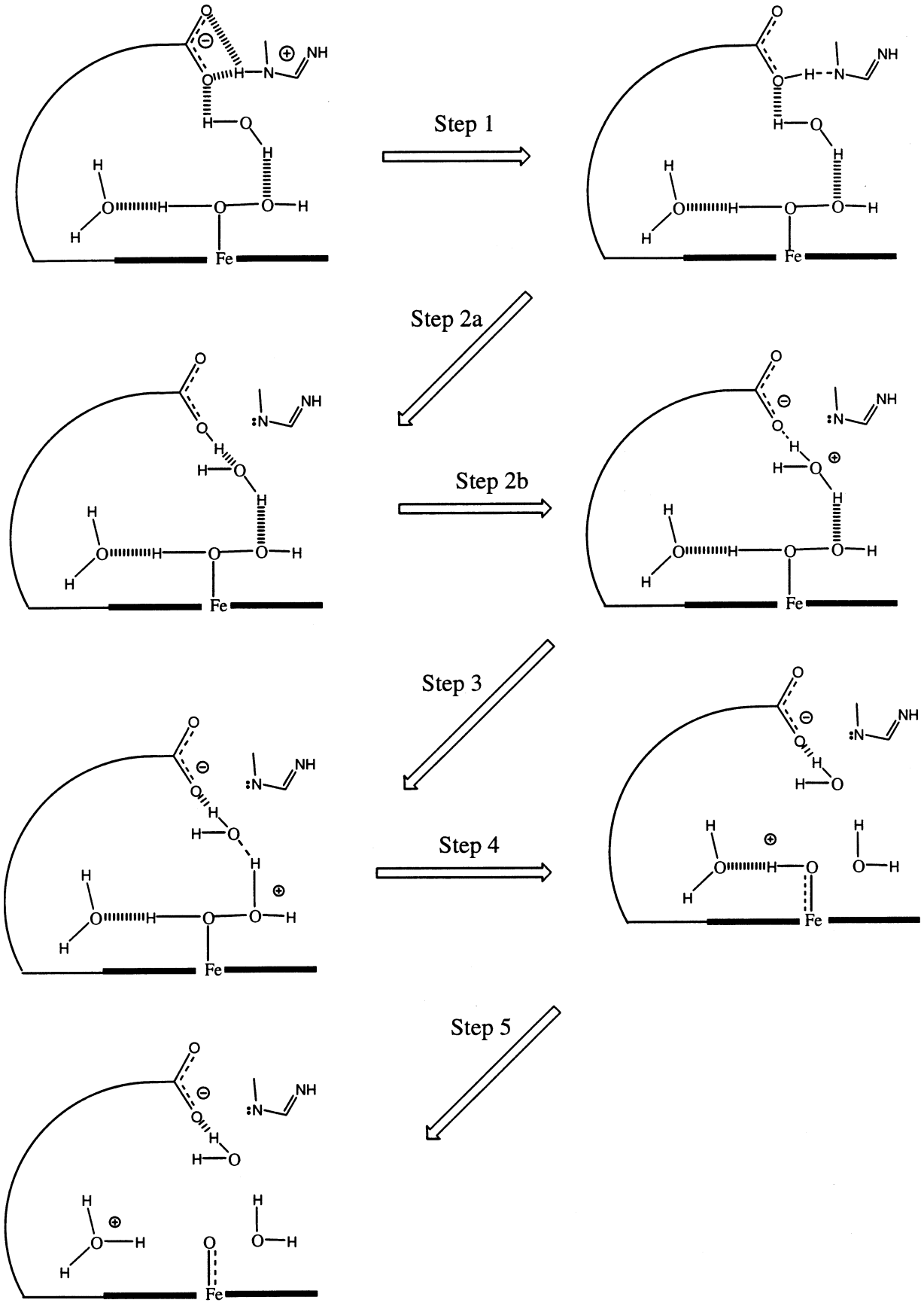

[a] Step 1: proton transfer from N_ϵ of His207 to an oxygen of the D-propionate. Steps 2a and 2b: the protonated propionate transfers a proton to a hydrogen-bonded water. Step 3: proton transfer from the H_3O^+ formed in step 2 to protonate the peroxide oxygen, O2, and begin O1−O2 bond scission. Step 5: proton transfer from H1 to a hydrogen-bonded water. (Steps 4 and 5 could be concerted or consecutive, as drawn.)

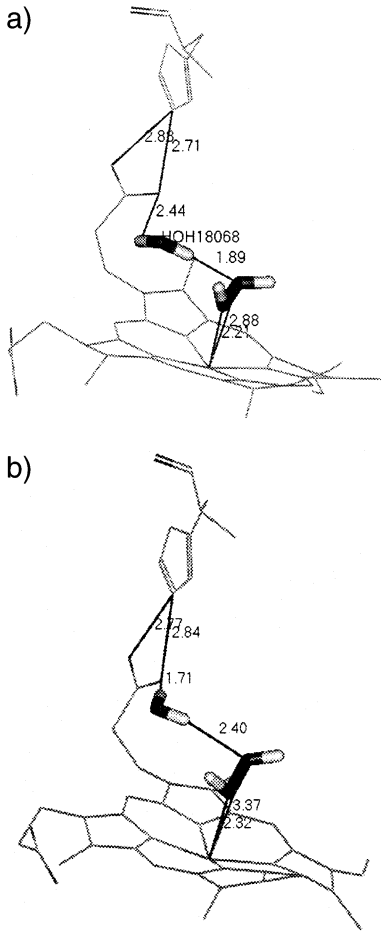

Figure 11. Positioning of the distal His207 relative to the heme propionate. The (protonated) distal His207 is hydrogen bonded to the heme propionate here, and typically, in the bifurcated pattern. The hydrogen bond is strong as judged from the heavy atom distances and it is persistent. The same propionate is also hydrogen bonded to W18068. The hydrogen bonding is from the peroxide O2 to a H of W18068. In this configuration, compound I formation is initiated by splitting off a water (see Scheme 3). (This contrasts with Figure 10a, where the hydrogen bond is from the peroxide H2 to W16085's O.) (a) The propionate to W18068 hydrogen bond is short whereas the W18068 to peroxide O2 hydrogen bond is long. (b) The propionate to W18068 hydrogen bond is long whereas the W18068 to peroxide O2 hydrogen bond is short. This motion is part of the proton shuttle.

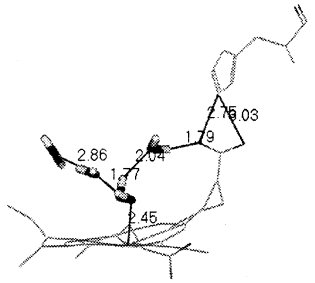

Figure 12. Same situation as for Figure 10 but about 150 ps later. There are two waters strongly hydrogen bonded to the peroxide H1 hydrogen. These waters are in turn hydrogen bonded to the bulk waters and serve to deprotonate O1.

ligand was assigned to be a water molecule, and this assignment resolves the ambiguity in the crystallographic data. The MD simulation carried out here shows that a water becomes the sixth ligand of the Fe when it is in the ferric heme state. The time it takes to ligate a water to the Fe is a strong function of the initial conditions of the simulation. Use of the XRAY initial condition, with its three waters within 8 Å of the Fe, leads to an attachment time of about 50 ps versus the MD initial condition with four waters within 8 Å of the Fe, where it is much faster, about 0.4 ps. One is tempted to conclude that XRAY water ligation should be slower than MD water ligation because the XRAY waters have been positioned to provide hydrogen bonds to residues (for example, W2473 is positioned to hydrogen bond to both the proximal His388 and Tyr504) whereas the MD method simply places the waters by excluding those that overlap the protein in the initial water lattice. However, the time of attachment also varies quite strongly with the startup protocol used. Constraining the protein atoms for different time intervals, and how the protein is heated by interaction with the solvent, influence the attachment time. Note that it is not one of the three waters within 8 Å of the Fe that becomes the ligand for the XRAY initial condition. What can be said with confidence is that there is a strong propensity of the heme Fe to bind a water forming a six-coordinate species, versus having waters trapped by residues or repelled from the vicinity of the Fe to prevent ligation.

MD simulations of the peroxidases cytochrome *c* peroxidase and isoenzyme C of horseradish peroxidase[18] along with crystallographic studies[8] have also found a stable water close to the Fe as well as an extensive hydrogen-bonding network in the heme vicinity. In PGHS-1, the distance from the heme to the bulk solvent is rather short.[25] That is convenient for the purposes of a MD simulation because it permits solvent to approach the heme on a time scale within the demands of the simulation that require having a large number of waters present. We find that the ligation of a water to the Fe is also associated with the movement of other waters, mostly into the distal side of the heme plane (top side in Figure 4). An exploration of how waters form hydrogen-bonded structures was made quantitative by the "tree" program we developed. Waters do form extensive hydrogen-bonding patterns that are connected to the stable Fe-ligated water. By examining all water trees that are longer than a certain number of links, and by using a definition of hydrogen bonding that varies from easy to hard, a sense of the stability and strength of these networks can be obtained. The data presented in the Results show that the bulk solvent is hydrogen bonded to a few waters that form a chain to connect to WL and, simultaneously, WL is hydrogen bonded to one or two more waters pointing toward the protein interior. The four to six waters that are strongly hydrogen bonded to WL are quite persistent, exchanging with other waters to form the same kind of networks on a broad time scale. Because substrates have to enter and leave the peroxidase site, there must be a combination of mobility, by exchange of a substrate with waters that lead from the bulk solvent to the heme, and stability, which permits a substrate to reside in the site for a sufficient time, to permit the formation of compound I.

The crystal structure suggests that there is a water hydrogen bonding to both proximal His388 and Tyr504. Raman spectroscopy of the peroxidase class of enzymes often shows a split Fe−His vibration[20,32−34] that is usually interpreted as a consequence of two populations: one with histidinate character and the other with a more basic character due to strong hydrogen bonding to an adjacent aspartate.[35] For PGHS-1 the suggestion is that this peak arises from the His388 being hydrogen bonded or not with the water that bridges this histidine and Tyr504.[20] The MD results in Figure 5 suggest that the bridging water does remain there, principally by its hydrogen bonding to Tyr504, and the hydrogen bond to His388 breaks and re-forms dynami-

cally. This would certainly lead to the observed broadening or splitting of the Fe−His vibrational band.

Mechanisms that have been proposed for compound I formation in peroxidases invoke an important role for a histidine and also an arginine residue in the vicinity of the heme.[12,13,16,17,36,37] The protonation state of the histidine is critical to these mechanisms because, if neutral, N_ϵ or N_δ protonated (charge 0), it can act as a proton acceptor (base) and, if cationic, both N_ϵ and N_δ protonated (charge +1), it can act as a proton donor (acid). Our simulations assume that the distal His207 has both N_ϵ and N_δ protonated. This assumption has critical consequences for a mechanistic scheme. His207's imidazole ring moves sufficiently far from the heme Fe, as shown in Figure 6, that it is an unlikely candidate for an acid/base reaction with the substrate. Conversely, a 400 ps simulation of PGHS-1, where the only change made was to use the neutral form of His207, reveals that now His207 remains close to its position in the X-ray structure. The (unprotonated) N_ϵ of His207 is about 4.5 Å from the Fe in the X-ray structure. The MD has this distance fluctuating between 4 and 5 Å over the 400 ps run. Thus, this one change has dramatic consequences to the structure of the heme "dome"—the α helix of residues on the distal side of the heme. Note that this latter simulation also has a water rapidly becoming the sixth ligand of the Fe. The distal histidine in peroxidases can be cationic or neutral, depending on the particular peroxidase and the system's pH.[8,17,37] The protonated form is naturally favored by acidic conditions. Biochemical studies indicate that His207 plays a critical role in supporting compound I formation in both PGHS-1[21] and PGHS-2.[38]

The movement of cationic His207 is a combination of a flipping up of the imidazole ring relative to its initial orientation and a shift in the backbone of the helix of which it is a member relative to the X-ray structure (cf. Figure 6). However, this α helix's structure is not significantly perturbed, as shown in Table 2. Once this shift occurs, the His207 obtains a stable structure where its N_ϵ is hydrogen bonded to the D-propionate oxygens. Most of the time, the hydrogen bonding is to both oxygens and the distance is close to "ideal" (around 2.8 Å) for this class of hydrogen bond.[31] This three-center hydrogen bonding can provide stabilization energy on the order of strong normal hydrogen bonds.[31] Hydrogen bonding between a histidine imidazole side chain and propionate oxygens has been ascribed a role in the structural stability of cytochrome *c* peroxidase[9,15,39] and is present in Myglobin.[40] In general, imidazole side chain hydrogen bonding to oxygen(s) of ionized residues such as aspartate plays an important role in providing structural stability of numerous enzymes.[41−43]

The introduction of hydrogen peroxide as a substrate for compound I formation was accomplished by mutating two waters into a hydrogen peroxide molecule. The waters chosen were the WL, the one that became the ligand to Fe, and a second water that eventually became hydrogen bonded to this water—WL = W8304 and W7655 for the XRAY initial condition. In this manner, we avoided the difficult computational task of diffusing in a ligand. Details of the accommodation of this ligand to the heme environment are given in the Results. For the purposes of the mechanism of compound I formation, the relevant issues are the stability and geometry of the peroxide binding to the Fe. The peroxide that forms is very stable. There is no tendency for it to dissociate from the Fe. Note that the sum of the charges on the oxygens of −0.8 is essentially the same as that on the water oxygen of −0.82 that it replaces. Although the charge is more diffuse, being spread over the two oxygens, its interaction with the Fe, and the constraints enforced by the surrounding residues and waters hydrogen bonded to the peroxide, are sufficient to keep it bound to the heme. The simulations carried out on horseradish peroxidase[17] find dominance by "end-on" (unequal O1 and O2 distances to the Fe) versus bridged peroxide oxygens. Examination of the roughly 500 ps of our data where the peroxide has been equilibrated shows that about half of the time the O1−Fe and O2−Fe distances are quite unequal and the dwell times are fluctuating between 10 and 80 ps. The motions can be characterized as rocking of the oxygens maintaining the orientation of the oxygens with respect to the heme plane and very occasional exchanges of the oxygens by rotation around the normal to the Fe-heme plane, as illustrated in Figures 8−10.

The steps for our mechanism for compound I formation are diagrammed in Scheme 3. The mechanism relies on there being a proton transport chain that spans His207, a propionate, a water molecule, and the peroxide. Step 1 is transfer of a proton from His207's N_ϵ hydrogen to an oxygen of the heme's D-propionate. The hydrogen bond between the N_ϵ hydrogen and the D-propionate is present all the time, once it is created, with essentially three-center hydrogen bonding to the two propionate oxygens dominating the configurations. Its formation requires the motion of the His207, as discussed in the Results and illustrated in Figures 6. Hydrogen bond formation between the cationic His207 and propionate oxygens is very favorable electrostatically. There is ample evidence for a cationic histidine−carboxylate hydrogen bond to be poised to do the proton transfer of step 1. That is, the equilibrium $A^+-H- - -B^- \leftrightarrow A- - -H-B$, where A^+ denotes acid (cationic histidine) and B^- denotes base (propionate), is not too far from either side. Furthermore, the barrier of the double well potential for proton motion between these two equilibrium configurations is not too large, so that the rate of proton transfer is relatively fast. Although solution p*K*'s are, of course, suspect within a protein, pK_a(propionic acid) = 4.87 and pK_b^+(histidine) = 6.0 are not very far apart. Thus, the system can be poised for proton transfer. Indeed, many studies of model propionic acid−aromatic amine complexes in a variety of solutions of differing dielectric constant exhibit tautomerism with the equilibrium constant not greatly different from unity. These studies also find that proton-transfer rate constants can be large.[44] Robust proton-transfer rates are favored by the heavy atom distance (here N_ϵ and propionate O) being relatively small (strong hydrogen bonds). The distance of around 2.8 Å in Figure 11 is typical of what we find and corresponds to strong hydrogen bonding. There is biochemical evidence for histidine−heme propionate hydrogen bonding and for tautomerism in these hydrogen bonds. For histidine aspartate hydrogen bonding the observation of a broadened Fe imidazole vibrational band containing two peaks suggests two possible states for the proton corresponding to proton tautomerism.[39] In cytochrome *c* oxidase,[45] where there are four propionates (because there are two hemes), a recent study presents evidence for one histidine propionate hydrogen bond having the proton covalently bonded to the histidine and another with the proton covalently bonded to the propionate (the proton has transferred). The particulars depend on the nearby metal's oxidation state. Thus, there is evidence for propionates being poised by the oxidation state of the metal (as well as by the nature of the surrounding residues, of course) for histidine-to-propionate proton transfer. In a more general context, the catalytic triads of the serine proteases[41] and cholinesterases,[46] and similar catalytic diads[42] involve a His···Asp(Glu) hydrogen bond that is known to be essential for catalytic activity. Recent work has characterized this hydrogen bonding

as short and strong.[41,42,46] In this case, either the tautomeric states are separated by a low barrier and can therefore interconvert readily or no such states are possible. Thus, a motif of a basic and an acidic residue providing tautomeric states with the ability to transfer a proton when needed may be quite general. We suggest that propionates can act as the acid partner for proton tautomerism.

Step 2 is a proton transfer from the carboxylic acid to a neighboring hydrogen-bonded water molecule. Figures 11 and 12 show that a water is hydrogen bonded to a D-propionate oxygen. A water at this position is quite stable. For example, W18068 is present and essentially always hydrogen bonded to the propionate for more than 300 ps. Proton transfer between the (weak) carboxylic acid and this water should be facile, even allowing for the hydrogen bonding of the propionate to the His207. This readily results in a re-formed propionate and H_3O^+. The remaining steps of the mechanism are similar to those proposed by Filizola and Loew for cationic His207.[17] The proton donor for step 3 in Scheme 3 is H_3O^+ whereas in their work it is the histidine itself. Certainly, H_3O^+ is a much better acid than a cationic histidine and this transfer should be essentially instantaneous. However, as we noted in the Results, not all the configurations of hydrogen bonding of the (now protonated) water that is hydrogen bonded to the O2 peroxide oxygen are correct geometrically. Only about 4−5% are properly aligned. Of course, once the water is protonated, this proportion can change. But, even with this restriction, productive configurations form sufficiently often to account for the observed rates of compound I formation.

Step 4 is the release of water from the peroxide−water complex. Loew has carried out ab initio calculations that conclude that this should be essentially a dissociative step.[36] Finally, step 5 releases the H1 proton of the peroxide oxygen to a hydrogen-bonded water molecule. As shown in Figure 12, H1 is hydrogen bonded to two waters. These waters are strongly hydrogen bonded and form a robust and persistent chain for removal of H1. In turn, these waters are hydrogen bonded to bulk waters in the usual fluctuating hydrogen-bonded pattern. The strong hydrogen bonders and their connection to the bulk provides a means to deprotonate O1 whenever it is required to do so by the relatively infrequent correct alignment of, e.g., W18068 with O2. To reset the system for the next catalytic event, HIS207 will be reprotonated, presumably from protons associated with bulk hydrogen-bonded water, though specific residues might also be involved.

V. Conclusions

Molecular dynamics simulations were performed on the resting and hydrogen peroxide-bound states of PGHS-1. We found that a water (WL) becomes the sixth ligand of the Fe(III) with the time of attachment dependent on the start up protocol used for the MD. Once (noncovalently) ligated, this WL persists as a ligand and becomes the "nucleus" for a hydrogen-bonded network of other water molecules. The network extends from the bulk solvent and funnels down to a chain of waters, on the distal side of the heme, that leads to WL. In turn, WL also hydrogen bonds to two other waters extending away from the bulk solvent. These hydrogen-bonding networks were analyzed for their extent, strength, and persistence. It is clear that, as in other peroxidases, hydrogen-bonded networks form in the heme's vicinity and can play a role in catalytic activity.

By combining WL and a water hydrogen bonded to it, a hydrogen peroxide molecule was constructed. The hydrogen peroxide was equilibrated to the protein and solvent and remains ligated to the Fe, with the peroxide in end-on configurations roughly half the time. Occasionally, the peroxide oxygens exchange their positions by rotation, a motion associated with a rearrangement of the surrounding hydrogen-bonded waters. The simulations of Filizola and Loew on HRPC−H_2O_2 complexes show similar behavior when the distal histidine is cationic.[17]

The stable ligation of H_2O and H_2O_2 to the Fe is based on the use of empirical MD potentials. In view of the importance of this interaction, it is gratifying that quantum mechanical studies also predict water and peroxide binding. Loew and Dupuis[36] used ab initio methods to evaluate the geometry and binding energy of H_2O_2 to protoporphyrin IX (with ring substituents replaced by H atoms) and imidazole (for histidine) and cite work to be published for the analogous calculation with H_2O. They found a stable complex with H_2O_2 and that the interaction with the Fe-heme is largely electrostatic in nature, thus favoring the utility of simple MD potentials. In view of the uncertainty in the MD electrostatic charges, especially on the Fe,[16,18,27] we tested various charges on the Fe (with compensation on the nitrogens) and found that water and peroxide still do bind.

We found that, due to a combination of the motion of (cationic) His207's imidazole ring and backbone, the N_ϵ carrying the potential proton donor to the peroxide moves sufficiently far away as to negate a direct His207 to peroxide proton donation mechanism of compound I formation. Instead, we found that the N_ϵ of His207 forms a hydrogen bond to the D-propionate oxygens, one of which is hydrogen bonded to a persistent water. This water is persistently hydrogen bonded to the peroxide with the water hydrogen acting as the donor to a peroxide oxygen about 5% of the time. We proposed that this provides a pathway for proton donation from His207 to the peroxide to initiate compound I formation. The small percentage of "correct" hydrogen-bonding configurations between the water and H_2O_2 does not preclude the formation of compound I. The rate of compound I formation is about 10^4-10^5 s^{-1} and, with 5% correct configurations, there are ample opportunities to provide the proton transfer of this step. The other steps in the mechanism should be very rapid.

The proposed mechanism relies on the presence of the propionates in the heme, in particular the D-propionate, as illustrated in Scheme 3. One way to test the proposed mechanism of compound I formation is to eliminate the possibility of interaction with the D-propionate. Replacing protoporphyrin IX by a heme lacking these substituents and assaying the enzyme's peroxidase activity may achieve this goal.

The protonation state of the distal histidine is crucial to the suggested mechanisms of compound I formation in heme peroxidases. At acid pH, the cationic form of the distal histidine of HRPC is favored, as determined by pH scan experiments.[37] The pK_a of the distal histidine in HRPC has been estimated between 4.0 and 8.7, depending on its environment.[47] The protonation state of H207 in PGHS-1 at physiological conditions had not been determined. An increase in the pK_a of histidine would be favored by nearby negatively charged residues.[48,49] It is interesting that the assumption of a cationic H207 leads, in the MD, to a configuration where it is hydrogen bonded to the propionate, indicating a consistency with this protonation state. A number of NMR spectroscopic studies have shown that it is not unusual to find *active-site* histidines with pK_a values that are larger than 7.[48,50,51] Thus, the possibility exists that the

peroxidase catalytic site in PGHS-1 supports a H207 with an elevated pK_a.

In an exploratory run of PGHS-1 with the distal His207 in its neutral form, as the only change, we found that the His207 remains close to the geometry found in the X-ray structure and that a water still becomes the sixth ligand of the heme. Work is in progress to again mutate this WL and a nearby water to form hydrogen peroxide and explore whether this neutral His207 will still remain sufficiently close to the peroxide to act as a proton acceptor and initiate compound I formation in this fashion.

Acknowledgment. The financial support of the National Institutes of Health (P01 GM57323) is gratefully acknowledged. R.I.C. thanks Professor W. L. Smith for many fruitful discussions concerning PGHS.

References and Notes

(1) Marnett, L. J.; Rowlinson, S. W.; Goodwin, D. C.; Kalgutkar, A. S.; Lanzo, C. A. *J. Biol. Chem.* **1999**, *274*, 22903.
(2) Smith, W. L.; DeWitt, D. L. In *Advances in Immunology*; Dixon, F. J., Ed.; Academic Press: San Diego, CA, 1996; Vol. 62, p 167.
(3) Smith, W. L.; Garavito, R. M.; DeWitt, D. L. *Annu. Rev. Biochem.* **2000**, *69*, 145.
(4) DeWitt, D. L. *Mol. Pharmacol.* **1999**, *4*, 625.
(5) Marnett, L. J.; Kalgutkar, A. S. *Curr. Opin. Chem. Biol.* **1998**, *2*, 482.
(6) Plount Price, M. L.; Jorgensen, W. L. *J. Am. Chem. Soc.* **2000**, *122*, 9455.
(7) Dunford, H. B. *Heme Peroxidases*; John Wiley and Sons Inc.: New York, 1999.
(8) Jones, P. J. *Biol. Chem.* **2001**, *276*, 13791.
(9) Smulevich, G. *Biospectroscopy* **1998**, *4*, 3.
(10) Dawson, J. H. *Science* **1988**, *240*, 433.
(11) Poulos, T. L. *J. Biol. Inorg. Chem.* **1996**, *1*, 356.
(12) Sono, M.; Roach, M. P.; Coulter, E. D.; Dawson, J. H. *Chem. Rev.* **1996**, *96*, 2841.
(13) Hiner, A. N. P.; Raven, E. L.; Thorneley, R. N. F.; Garcia-Canovas, F.; Rodriguez-Lopez, J. N. J. *Inorg. Biochem.* **2002**, *1*, 0000.
(14) Tsai, A.; Wei, C.; Baek, H. K.; Kulmacz, R. J.; Wart, H. E. V. *J. Biol. Chem.* **1997**, *272*, 8885.
(15) Finzel, B. C.; Poulos, T. L.; Kraut, J. *J. Biol. Chem.* **1984**, *259*, 13027.
(16) Collins, J. R.; Du, P.; Loew, G. H. *Biochemistry* **1992**, *31*, 11166.
(17) Filizola, M.; Loew, G. H. *J. Am. Chem. Soc.* **2000**, *122*, 18.
(18) Banci, L.; Carloni, P.; Savellini, G. G. *Biochemistry* **1994**, *33*, 12356.
(19) De Gioia, L.; Fantucci, P. *J. Mol. Struct. (THEOCHEM)* **1999**, *469*, 41.
(20) Seibold, S. A.; Cerda, J. F.; Mulichak, A. M.; Song, I.; Garavito, R. M.; Arakawa, T.; Smith, W. L.; Babcock, G. T. *Biochemistry* **2000**, *39*, 6616.
(21) Shimokawa, T.; Smith, W. L. *J. Biol. Chem.* **1991**, *266*, 6168.
(22) van Gunsteren, W. F.; Berendsen, H. J. C. GROMOS Manual, 1987.
(23) Hockney, R. W.; Eastwood, J. W. *Computer simulation using particles*; McGraw-Hill: New York, 1981.
(24) Allen, M. P.; Tildesley, D. J. *Computer Simulation of Liquids*; Clarendon Press: Oxford, U.K., 1987.
(25) Picot, D.; Loll, P. J.; Garavito, R. M. *Nature* **1994**, *367*, 243.
(26) Walters, P.; Stahl, M. Babel 1.6, 1992.
(27) Soares, C. M.; Martel, P. J.; Mendes, J.; Carrondo, M. A. *Biophys. J.* **1998**, *74*, 1708.
(28) Halgren, T. A. J. *Comput. Chem.* **1996**, *17*, 616.
(29) Hunt, R. H.; Leacock, R. A.; Peters, C. W.; Hecht, K. T. J. *Chem. Phys.* **1965**, *42*, 1931.
(30) Meredith, C.; Hamilton, T. P.; H. F. S., III. *J. Chem. Phys.* **1992**, *96*, 9250.
(31) Jeffrey, G. A.; Saenger, W. *Hydrogen Bonding in Biological Structures*; Springer-Verlag: Berlin, 1991.
(32) Smulevich, G.; Hu, S.; Rodgers, K. R.; Goodin, D. B.; Smith, K. M.; Spiro, T. G. *Biospectroscopy* **1996**, *2*, 365.
(33) Nissum, M.; Neri, F.; Mandelman, D.; Poulos, T. L.; Smulevich, G. *Biochemistry* **1998**, *37*, 8080.
(34) Lou, B.-H.; Snyder, J. K.; Marshall, P.; Wang, J.-S.; Wu, G.; Kulmacz, R. J.; Tsai, A.-L.; Wang, J. *Biochemistry* **2000**, *39*, 12424.
(35) Sinclair, R.; Hallam, S.; Chen, M.; Chance, B.; Powers, L. *Biochemistry* **1996**, *35*, 15120.
(36) Loew, G.; Dupuis, M. *J. Am. Chem. Soc.* **1996**, *118*, 10584.
(37) Rodriguez-López, J. N.; Lowe, D. J.; Hernández-Ruiz, J.; Hiner, A. N. P.; Garcia-Cánovas, F.; Thorneley, R. N. F. *J. Am. Chem. Soc.* **2001**, *123*, 11838.
(38) Landino, L. M.; Crews, B. C.; Gierse, J. K.; Hauser, S. D.; Marnett, L. J. *J. Biol. Chem.* **1997**, *272*, 21565.
(39) Smulevich, G.; Miller, M. A.; Kraut, J.; Spiro, T. G. *Biochemistry* **1991**, *30*, 9546.
(40) Peterson, E. S.; Friedman, J. M.; Chien, E. Y. T.; Sligar, S. G. *Biochemistry* **1998**, *37*, 12301.
(41) Cassidy, C. S.; Lin, J.; Frey, P. A. *Biochemistry* **1997**, *36*, 4576.
(42) Schultz, L. W.; Quirk, D. J.; Raines, R. T. *Biochemistry* **1998**, *37*, 8886.
(43) Kim, Y.; Ahn, K.-H. *Theo. Chem. Acc.* **2001**, *106*, 171.
(44) Zeeger-Huyskens, T.; Huyskens, P. In *Molecular Interactions*; Ratajczak, H., Orville-Thomas, W. J., Eds.; Wiley: New York, 1980; Vol. 2, p 1.
(45) Behr, J.; Michel, H.; Mäntele, W.; Hellwig, P. *Biochemistry* **2000**, *39*, 1356.
(46) Viragh, C.; Harris, T. K.; Reddy, P. M.; Massiah, M. A.; Mildvan, A. S.; Kovach, I. M. *Biochemistry* **2000**, *39*, 16200.
(47) Rodriguez-Lopez, J. N.; George, S. J.; Thorneley, R. N. F. *J. Biol. Inorg. Chem.* **1998**, *3*, 44.
(48) Tishmack, P. A.; Bashford, D.; Harms, E.; VanEtten, R. L. *Biochemistry* **1997**, *36*, 11984.
(49) Kahyaoglu, A.; Jordan, F. *Protein Sci.* **2002**, *11*, 965.
(50) Liu, T.; Ryan, M.; Dahlquist, F. W.; Griffith, O. H. *Protein Sci.* **1997**, *6*, 1937.
(51) Ryan, M.; Liu, T.; Dahlquist, F. W.; Griffith, O. H. *Biochemistry* **2001**, *40*, 9743.